How to Cite: Ryabykh, A.V., Maslova, O.A., & Beznosyuk, S.A. (2023). Mechanisms of Docking of Superoxide Ions in the Catalytic Cycle of Manganese and Iron Superoxide Dismutases. *Eurasian Journal of Chemistry, 111(3), 104-113.* https://doi.org/10.31489/2959-0663/3-23-4

Article

Received: 04 April 2023 | Revised: 22 May 2023 |
Accepted: 15 June 2023 | Published online: 26 July 2023

UDC 544.18+544.431+544.476.2 https://doi.org/10.31489/2959-0663/3-23-4

Andrey V. Ryabykh, Olga A. Maslova, Sergey A. Beznosyuk*

Department of Physical and Inorganic Chemistry, Altai State University, Barnaul, Russia
*(*Corresponding author's e-mail: bsa1953@mail.ru)*

Mechanisms of Docking of Superoxide Ions in the Catalytic Cycle of Manganese and Iron Superoxide Dismutases

In this paper, we propose an approach to resolving some questions about the catalytic action of manganese and iron superoxide dismutases. At the level of a pure quantum-chemical calculation using an ORCA 5.0.3 program, a PBE functional and a def2-SVP and def2-TZVP basis sets, the possible mechanisms of superoxide ions binding to the active sites of enzymes, the electron transfer distances and their characteristics were established. It is shown that the initial form of the fifth ligand in both active sites is the hydroxide ion OH^-. Before the primary electron transfer, active sites are protonated, the hydroxide ion is converted into a water molecule H_2O. Primary electron transfers from the superoxide ion to Mn^{3+}-SOD and Fe^{3+}-SOD occur by the associative mechanism, with the formation of an octahedral complex, at a transfer distance of 1.95 Å and 2.56 Å, respectively. At the second stage, the superoxide ion accepts the electron by the substitution mechanism from Mn^{2+}-SOD at the transfer distance of 2 Å to form bonds with the water molecule and a tyrosine. The superoxide ion accepts the electron from Fe^{2+}-SOD through the outer-sphere mechanism, where it binds to a histidine and the water molecule at the transfer distance of 4.24 Å.

Keywords: manganese superoxide dismutase, iron superoxide dismutase, electron transfer, computer simulation, density functional theory, catalytic mechanism.

Introduction

In the course of metabolic transformations in a living organism, oxygen O_2 is able to turn into extremely reactive particles — reactive oxygen species (ROS). One of the first in the sequence of formation of free radicals is the superoxide ion O_2^-. Their accumulation can adversely affect the state of cellular components, destroying them and leading to various diseases of the body as a whole [1]. In a healthy body, antioxidants and antioxidant enzymes provide protection against excessive ROS production. Enzymes of the superoxide dismutase (SOD) group ensure the neutralization of superoxide ions O_2^- to molecular oxygen O_2 and hydrogen peroxide molecules H_2O_2. These enzymes contain 3d-metals (for example, Mn-SOD considered in this study contains Mn^{3+} ion and Fe-SOD contains Fe^{3+} ion). In the first half of the catalytic cycle, the SOD active site takes one electron from the superoxide ion, while the Me^{3+} ion is reduced to Me^{2+}. In the second half of the catalytic cycle, the SOD active site donates one electron to the superoxide ion, while the Me^{2+} ion is oxidized to Me^{3+} [2, 3]. Manganese superoxide dismutase is present in all eukaryotic organisms. It is contained in the mitochondrial matrix, where ROS are directly formed. Thus, Mn-SOD is one of the first steps in the antioxidant protection of cell components [4]. Iron superoxide dismutase is found mainly in prokaryotes [5]. It is noteworthy that the active sites of manganese and iron superoxide dismutases have the same structure.

At the moment, some questions regarding the mechanism of ROS neutralization by these superoxide dismutases still remain debatable. There are reasons for this that somewhat limit direct experimental studies. It is noted that these reasons are the extremely high rate of the catalytic reaction, the low half-life of the superoxide ion in an aqueous-protein medium, and the difficulty in detecting protons and protonated amino acid residues. The corresponding problems are covered in the review article [4]. Since more stable azide ions N_3^- are often used instead of them in studies of the mechanisms of reactions involving superoxide ions O_2^-, the question remains whether the superoxide ion and the metal ion are directly bound during electron transfer, or whether the transfer proceeds at a long distance with the participation of ligands. In addition, there are controversial points regarding the conditions for the participation of protons in this reaction, since their presence is important in the second stage, where hydrogen peroxide is formed from the superoxide ion. There are the following questions. At what distance do electron transfers occur? What is the nature of the fifth ligand

attached to the metal ion during electron transfers: a hydroxide ion or a water molecule? When does the first proton transfer occur: before the primary electron transfer or after? What is the main source of the proton in electron transfers?

In this study, the authors propose a solution to these issues based on computer simulation using a pure quantum chemical method. Since manganese and iron superoxide dismutases have the same structure of the active center, it is possible to compare the role of the nature of the metal ion in the efficiency of ROS neutralization. Methods for docking the superoxide ion and the active center of manganese and iron superoxide dismutase were studied with an estimate of the electron transfer distance at two stages of catalytic cycles. The thermodynamic and kinetic characteristics of electron transfers are obtained according to the Marcus transfer theory [6].

Computational Details

Modeling was carried out using the ORCA software package version 5.0.3 [7]. As a calculation method, we used the level of density functional theory using the GGA density functional of Perdew–Burke-Ernzerhof PBE [8]. The def2-TZVPD basis set [9] was used to optimize the geometry and calculate single point energies of small particles (O_2^-, O_2, HO_2, HO_2^-, H_2O, H_3O^+). When optimizing the geometry of the active site, a simplified def2-SVP basis [9] was used with additional restrictions in the form of pinning 8 hydrogen atoms of the methyl groups to simulate the fact that the active site is retained by the protein environment [10]. After geometry optimization, the single point energy of the active site structure was calculated with the def2-SVPD basis. In addition, in all cases, when calculating the active site, the oxygen atoms O, manganese Mn, and iron Fe were always subject to the def2-TZVPD basis set. In any calculation, to take into account fine dispersion interactions, the atomic pair dispersion correction algorithm based on rigidly coupled partial charges D4 was used [11]. The influence of the dielectric medium was taken into account using the CPCM continuum model. The surface type is Gaussian VdW [12]. Since the active sites in the protein are located in the solvent access zone, the corresponding values of the dielectric constant and refractive index of water were taken as parameters of the solvent model ($\varepsilon = 80{,}4$; $n = 1{,}333$).

Figure 1 shows a structure of the active site of the enzymes that were modeled. The proposed sources of the proton during the secondary electron transfer are indicated there. Position 4, which is an external solvent, is not shown in the figure. Two histidine ligands (His) and one aspartate ion (Asp) are in equatorial positions. The third His and the aqueous ligand are in axial positions. The aqueous ligand can be either a hydroxide ion OH^- or the water molecule H_2O. The second coordination sphere contains the amino acid tyrosine (Tyr).

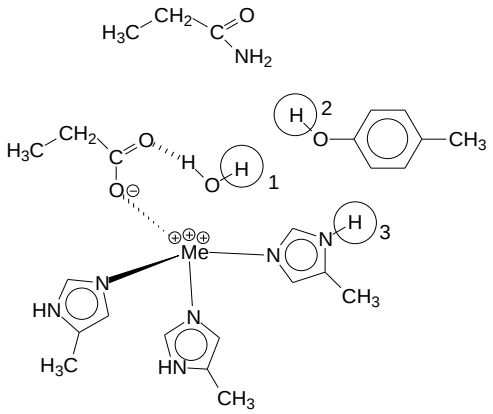

1 — proton of the water molecule; *2* — proton of the hydroxyl group;
3 — proton of the histidine ligand. Me = Mn, Fe

Figure 1. Proton sources in the Me-SOD active site

The electron transfer distances *R* and the corresponding Marcus transfer rate constants k_{obs} served as the main selection criteria for a possible mechanism of superoxide ion binding to active sites. Estimating the electron transfer distance is often a rather non-trivial task, and often this value is introduced, for example, by fitting. In this work, the following approach was used. The transfer distance *R* was estimated by constructing the potential energy surface (PES) profile when donor D and acceptor A approached each other. For the systems under consideration (oxygen–superoxide dismutase), the variable distance was the distance between the

active form of oxygen and the metal atom (Mn, Fe). The points of local minima on the PES were taken as the transfer distance. Under the conditions of being in the energy minimum, the system can stay longer. Therefore, the probability of electron transfer increases when the electron terms of the donor and acceptor cross. However, only the energy minimum is not a sufficient condition, since there can be several such extrema on one PES. An analysis of the spin population of atoms according to Mulliken can serve as a sufficient criterion for selecting the required minimum. We plotted the functions of the dependence of the difference between the spin populations of the donor and acceptor on the distance. The combination of minima on the PES and a sharp change in the function of the population difference gave the estimated transfer distance *R*. This study considers three variants of the superoxide ion docking mechanism. The first is associative, in which the superoxide ion enters the first coordination environment of the metal to form an octahedral structure. The second is substitutional, in which the superoxide ion enters the first coordination environment of the metal and replaces one of the five ligands. The third is outer-sphere, in which the superoxide ion combines with one of the ligands without forming a bond with the metal ion.

The rate constant of the Marcus second-order electron transfer reaction *k* was estimated using the following equation [6]:

$$k = k_{et} \cdot K_{pre}^{\neq} = \frac{8 \cdot \pi^3}{3 \cdot h} \cdot \frac{H_{DA}^2}{\sqrt{\pi \cdot \lambda_{tot} \cdot k_B \cdot T}} \cdot N_A \cdot R^3 \cdot \exp\left(-\frac{\Delta G^{\neq} + W_R}{k_B \cdot T} \right), \quad (1)$$

where *h* — the Planck's constant, J·s; H_{DA} — an electronic interaction matrix element, J; λ_{tot} — a total energy of the system reorganization, J; k_B — the Boltzmann constant, J/K; *T* — the temperature, K; N_A — the Avogadro constant, mol^{-1}; *R* — the electron transfer distance, dm; $\Delta G^{\neq}$ — the transfer activation energy, J; W_R — an electrostatic work of convergence of donor and acceptor, J.

The algorithm for estimating the quantities H_{DA}, λ_{tot}, $\Delta G^{\neq}$ and W_R is given in the article [13].

Equation (1) is suitable for the case when the electronic terms intersect insignificantly, the matrix element H_{DA} has values of the order of $1.5 \cdot k \cdot T$, and the electron transfer proceeds non-adiabatically. If the electronic terms overlap significantly, then an adiabatic splitting of the PES occurs. In this case, it is preferable to calculate the electron transfer rate constant using the following equation [14]:

$$k^{AD} = k_{et}^{AD} \cdot K_{pre}^{\neq} = \frac{\nu \cdot \varepsilon}{3 \cdot n^2} \cdot \sqrt{\frac{\pi \cdot \lambda_{tot}}{k_B \cdot T}} \cdot N_A \cdot R^3 \cdot \exp\left(-\frac{\Delta G^{\neq} + W_R}{k_B \cdot T} \right), \quad (2)$$

where *v* — the solvent nuclear reorganization rate = $1.25 \cdot 10^{11}$ s^{-1} (at 298.15 K); ε — the solvent dielectric constant; *n* — the solvent refractive index.

The donor and acceptor radii used in the calculation of the energy of reorganization and electrostatic work are also ambiguous from the point of view of their estimation. The radius of an oxygen-containing particle is estimated as the sum of half of the O–O bond length and the radius of an oxygen atom. The radius of the active site strongly depends on the distance *R* and is estimated in each case separately for the atoms atomic orbitals of which are involved in the formation of the molecular orbital involved in electron transfer. For the cases of associative and substitutional mechanisms, where *R* is less than 3 Å, the covalent radii of atoms were taken (0.66 Å for O and 0.71 Å for N [15]). For the case of the outer sphere mechanism, the van der Waals radii of atoms were taken (1.55 Å for O and 1.60 Å for N [16]).

The electron transfer accompanies the diffusion of reactants to each other. Therefore, the experimentally observed value of the rate constant k_{obs} of the catalytic process is a combination of the second-order rate constants *k* of electron transfer and diffusion of reactants k_{diff} [17]:

$$k_{obs} = \frac{k \cdot k_{diff}}{k + k_{diff}}, \quad (3)$$

where *k* — the rate constant of the Marcus second-order electron transfer reaction, $M^{-1} \cdot s^{-1}$; k_{diff} — the diffusion rate constant of transfer reagents, $M^{-1} \cdot s^{-1}$.

The constant k_{diff} in the continuum solvent model can be estimated using the Smoluchowski equation [18]:

$$k_{diff} = 4 \cdot \pi \cdot N_A \cdot (D_D + D_A) \cdot (r_D + r_A), \quad (4)$$

where *D* — a diffusion coefficient, $m^2 \cdot s^{-1}$; *r* — the radii of the reactants, m.

At *T* = 298.15 K in the aqueous medium for an oxygen-containing particle $D = 2.1 \cdot 10^{-9}$ m^2/s [17]. *D* for the active site as a massive slow-moving particle is taken as 0. Based on *k* and k_{diff}, the observed electron transfer rate constant k_{obs} is calculated.

To assess the intermolecular and coordination bonds of atoms, the topological analysis of the electron density according to Bader was used in the framework of the QTAIM theory of atoms in molecules. Based on the results of the topological analysis, the bond critical points (3; –1) were identified and the values of the electron density ρ and the Laplacian of the electron density Δρ at these points were calculated using the Multiwfn 3.8 software package [19]. For the topological analysis of the electron density, the following designations of atoms are introduced here. The ligand containing the N^1 atom is axial in the trigonal bipyramid and is located opposite the hydroxide ion. Ligands containing N^2 and N^3 atoms are equatorial and located opposite the aspartate ligand.

Results and Discussion

The results of this study showed that the high-spin structures of active sites are the most stable. Thus, the active site of Mn^{3+}-SOD in the oxidized form due to Mn^{3+} has a quintet state, and the active site of Fe^{3+}-SOD in the oxidized form due to Fe^{3+} has a sextet state. In the reduced form, the Mn^{2+}-SOD and Fe^{2+}-SOD active sites have sextet and quintet states, respectively.

Consider the first half of the catalytic cycle. Here, the superoxide ion is the electron donor and the superoxide dismutase active site is the electron acceptor. In the oxidized original form of these enzymes, the first coordination environment of the metal contains the hydroxyl ion OH^-. During the catalytic process, this ligand can be replaced by the water molecule. What form of the active site is an electron acceptor: with an OH^- or H_2O ligand? Let us consider two options for the implementation of the primary electron transfer. In the first variant, the electron acceptor will be the active site, where the ligand for the metal ion is the hydroxide ion. In this case, the change in the Gibbs function of primary electron transfer for active centers is ΔG^0(Mn) = +0.434 eV and ΔG^0(Fe) = +0.014 eV. Positive values indicate that the interaction of the superoxide ion with the active site in the presence of the hydroxide ion is thermodynamically unfavorable. In the second case, the electron acceptor will be the active site, where the ligand for the metal ion is the water molecule. In this case, the change in the Gibbs function of primary electron transfer for active sites is ΔG^0(Mn) = –0.695 eV and ΔG^0(Fe) = –1.109 eV. Strongly negative values indicate that the interaction of the superoxide ion with the active site in the presence of a water molecule is thermodynamically favorable. Based on these data, it can be concluded that before the primary electron transfer, a proton transfer occurs, while it attaches to the hydroxide ion to form the water molecule. The source of the proton is the hydronium ion from the solvent.

Next, we consider the interaction of the superoxide ion with the transfer of an electron to the active site of manganese and iron superoxide dismutases. The attack of the low-molecular particle occurred from the side of the solvent, where in the natural form of the protein, no atoms prevented the passage of the ion to the metal. In Figure 2, under (*a)*, the potential energy curves of the approach of the superoxide ion O_2^- to the manganese ion Mn^{3+} and the corresponding differences in spin population are shown, and under (*b*), the energies of the approach of the superoxide ion O_2^- to the iron Fe^{3+} ion and the corresponding differences in the spin population are shown.

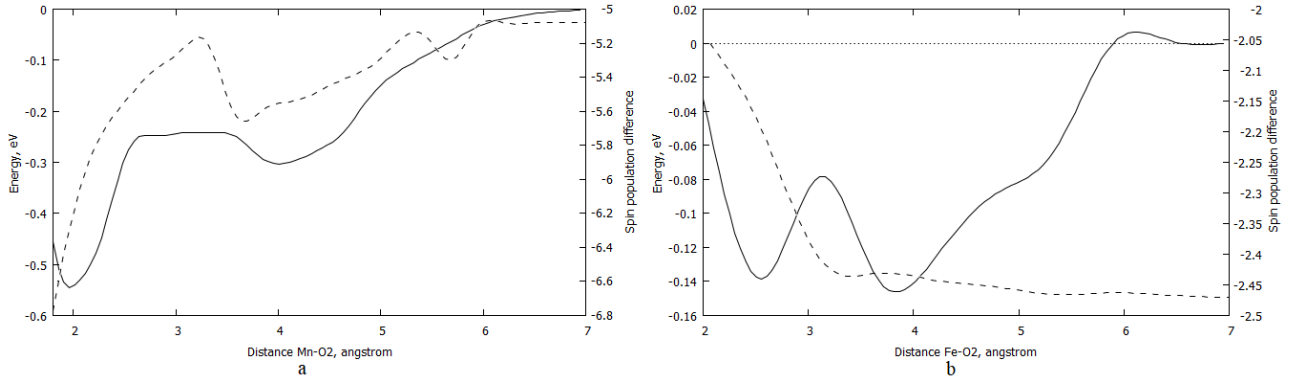

a — manganese Mn^{3+} ion; *b* — iron Fe^{3+} ion

Figure 2. Curves of the potential energy of the interaction between the superoxide ion O_2^- and the active site of superoxide dismutase (left y-axis and solid line) and the corresponding spin population differences (right y-axis and dashed line)

For the case with the manganese active site, two minima are observed. The first at R_1 = 4.1 Å is due to the interaction of the superoxide ion and the water molecule. The most stable and characteristic minimum is observed at R_2 = 1.95 Å. The superoxide ion enters the first coordination sphere of manganese. In this case, the trigonal-bipyramidal coordination will change to octahedral. A sharp change in the spin population difference starts from 3.2 Å. This coincides with the equilibrium distance of 1.95 Å. The most probable electron transfer distance is in the vicinity of this minimum. This allows us to discard the outer-sphere and substitution mechanisms and consider only the associative mechanism of electron transfer. The acceptor radius r_A is estimated as the sum of the distance from the manganese atom to the hydroxide ion (2.157 Å) and the covalent radius of the oxygen atom (0.66 Å).

For the case with the iron active site, stable and characteristic minima are observed at R_1 = 3.8 Å and R_2 = 2.6 Å. A sharp change in the spin population difference starts from 3.3 Å. This coincides with the equilibrium distance of 2.6 Å. The most probable electron transfer distance is in the vicinity of this minimum. The superoxide ion enters the first coordination sphere of iron. In this case, the trigonal-bipyramidal coordination will change to octahedral. This interaction does not imply substitution and outer sphere mechanisms. The reason may be the very nature of the water ligand. With the manganese ion Mn^{3+}, after the formation of the water molecule, the proton goes to Asp. As a result, the hydroxide ion OH^- is there, which, as the superoxide ion approaches, again acquires a proton from the Asp ligand. Further, this proton oscillates between the oxygen of the water and the oxygen of the superoxide ion, providing additional stabilization of the system. With an iron ion, this phenomenon is not observed. The acceptor radius r_A is estimated as the sum of the average distance from the iron atom to nitrogen atoms (2.012 Å) and the covalent radius of the nitrogen atom (0.77 Å). Table 1 shows changes in the Gibbs functions ΔG^0, reorganization energy λ_{tot}, and activation energy $\Delta G^{\neq}$, as well as estimates of the first and second order electron transfer rate constants in the framework of the Marcus paradigm for the primary electron transfer from the superoxide ion to the active site. The rate constants are given for non-adiabatic and adiabatic calculation options. The preferred option is in bold.

Table 1

Kinetic and thermodynamic characteristics according to Marcus of the primary electron transfer from the superoxide ion to the Me-SOD active site

Parameter	Association mechanism	
	Mn-SOD	Fe-SOD
ΔG^0, eV	–0.695	–1.109
r_D, Å	1.337	1.337
r_A, Å	2.817	2.648
R, Å	1.95	2.56
λ_{tot}, eV	1.840	2.114
$\Delta G^{\neq}$, eV	0.065	0.015
H_{DA}, eV	0.0861	0.2038
k_{diff}, $M^{-1}\cdot s^{-1}$	$2.02\cdot10^9$	$2.02\cdot10^9$
k_{et} (k_{et}^{AD}), s^{-1}	$7.29\cdot10^{12}$ (**$7.18\cdot10^{11}$**)	$2.64\cdot10^{14}$ (**$5.34\cdot10^{12}$**)
k (k^{AD}), $M^{-1}\cdot s^{-1}$	$4.14\cdot10^{13}$ (**$4.08\cdot10^{12}$**)	$2.59\cdot10^{15}$ (**$5.24\cdot10^{13}$**)
k_{obs} (k_{obs}^{AD}), $M^{-1}\cdot s^{-1}$	$2.02\cdot10^9$ (**$2.02\cdot10^9$**)	$2.02\cdot10^9$ (**$2.02\cdot10^9$**)

Transitions in Mn^{3+}-SOD-O_2^- are transitions between the quartet ground (Q0) and quartet first (Q1) states. Unlike Fe^{3+}-SOD-O_2^-, Mn^{3+}-SOD-O_2^- transfer involves α-electrons. The unpaired electrons of the Mn^{3+}-SOD active center and the O_2^- superoxide ion have oppositely directed spins. The transition in Fe^{3+}-SOD-O_2^- is a transition between the septet ground (H0) and septet first excited (H1) states. All interactions are adiabatic due to the high value of the H_{DA} matrix element.

It is noteworthy that the inner-sphere reorganization energy is 2 times lower for Fe^{3+}-SOD than for Mn^{3+}-SOD, which is associated with smaller structural perturbations after the primary electron transfer. But at the same time, the outer-sphere reorganization energy is higher for Fe^{3+}-SOD. The reactions of electron transfer from superoxide ions to the active site of manganese and iron superoxide dismutases by the associative mechanism proceed in the diffusion mode. The primary electron transfer in the case of iron superoxide dismutase is an order of magnitude faster than in the case of manganese superoxide dismutase.

Thus, the primary electron transfer from the superoxide ion to the active site of Mn^{3+}-SOD and Fe^{3+}-SOD proceeds according to the associative mechanism with the formation of an octahedral coordination of

the metal ion. This indicates a high chemical affinity between the negatively charged superoxide ion and the positively charged metal ion. The metal ion exerts a strong polarizing effect on the superoxide ion and detaches an electron from it. Next, we consider the features of the behavior of the electron density at the bonding critical points of the complex of the superoxide ion and the Me-SOD active site in various versions of the mechanism of binding the superoxide ion and the metal (Table 2).

Table 2

Critical bonding points (3; –1) for primary electron transfer in the Me-SOD donor-acceptor complex. Parameters ρ and Δρ are expressed in atomic units

Bond	Parameter	Associative mechanism	
		Mn-SOD	Fe-SOD
Me–N^1	ρ	0.0790	0.0709
	Δρ	+0.302	+0.282
Me–N^2	ρ	0.0737	0.0709
	Δρ	+0.275	+0.266
Me–N^3	ρ	0.0540	0.0705
	Δρ	+0.191	+0.284
Me–O^{Asp}	ρ	0.0704	0.0846
	Δρ	+0.293	+0.381
Me–H_2O	ρ	0.0598	0.0596
	Δρ	+0.234	+0.241
Me–O_2^-	ρ	0.1002	0.0244
	Δρ	+0.382	+0.075

The Mn–N^3 bond, which is located perpendicular to the Mn–O_2 bond in the octahedron, is strongly weakened. In other bonds, the share of ionicity increases. Since the superoxide ion in the octahedral Fe-SOD complex is located at a greater distance than in the Mn-SOD complex, it has less effect on other iron ligands. The Fe–Asp bond is weakened the most. The superoxide ion is much more strongly bound to the Mn^{3+} ion than to the Fe^{3+} ion.

Consider the second half of the catalytic cycle. Here, the active site Me^{2+}-SOD acts as a donor, and the superoxide ion O_2^- acts as an acceptor. The secondary electron transfer, like the primary one, is complicated by the coupled proton transfer. In view of the instability of the peroxide ion O_2^{2-} in an aqueous medium, it makes sense to assume that prior to electron transfer, a proton is transferred to the superoxide ion O_2^-, and the hydroperoxide radical $HO_2\cdot$ is formed [13].

In the Mn-SOD and Fe-SOD active sites, there are several variants of the proton source that attaches to the superoxide ion after it is attached to the active site. They are shown in Figure 1. We have four main sources of the proton. 1. A proton is split off from the water molecule, which is in the first ligand environment of the Me^{2+} ion. 2. The proton is split off from the hydroxyl group from the phenol residue, which is in the second ligand environment of the Me^{2+} ion. 3. The proton is split off from the nitrogen atom of the histidine residue, which is in the first ligand environment of the Me^{2+} ion. 4. The proton joins the O_2^- ion in a place outside the active site. Consider the energy of protonation ΔG_{pr} followed by electron transfer ΔG^0. These data are presented in Table 3.

Table 3

Protonation (ΔG_{pr}) and secondary electron transfer (ΔG^0) energies in Me-SOD

Source	1	2	3	4
Mn^{2+}-SOD				
ΔG_{pr}, eV	+0.692	+0.369	+0.356	–
ΔG^0, eV	–0.927	+0.236	+0.072	+0.202
Fe^{2+}-SOD				
ΔG_{pr}, eV	+0.647	+0.384	+0.360	–
ΔG^0, eV	–0.508	+0.151	+0.353	+0.616

It can be seen that protonation of superoxide from the water molecule (source 1) is most advantageous, followed by electron transfer to the hydroperoxide radical $HO_2\cdot$. In this case, the water molecule is converted into the hydroxide ion OH^-.

Next, we consider the interaction of the superoxide ion with electron transfer from the active site of manganese and iron superoxide dismutases to the hydroperoxide radical. In Figure 3, under (*a*), the potential energy curves of the approach of the superoxide ion O_2^- to the manganese ion Mn^{2+} and the corresponding differences in spin population are shown, and under (*b*), the energies of the approach of the superoxide ion O_2^- to the iron Fe^{2+} ion and the corresponding differences in the spin population are shown.

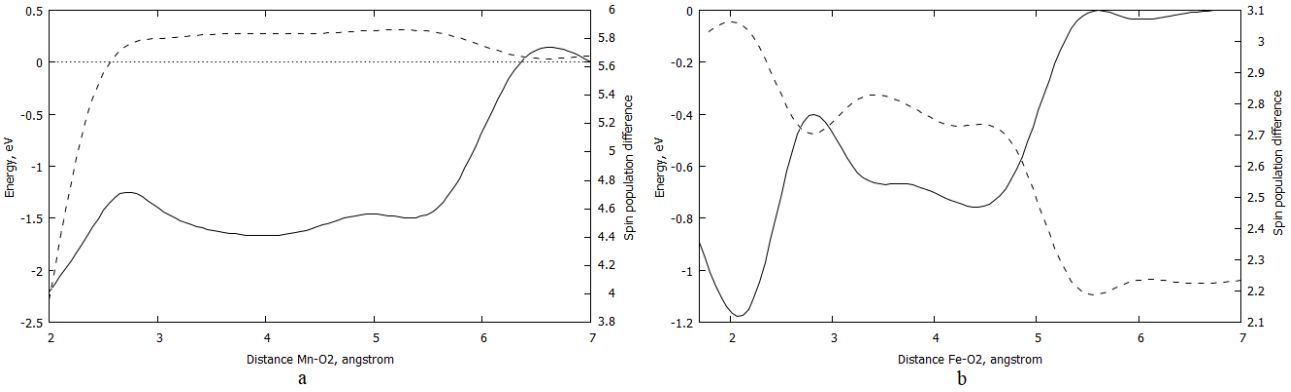

a — manganese Mn^{2+} ion; *b* — iron Fe^{2+} ion

Figure 3. Curves of the potential energy of the interaction between the superoxide ion O_2^- and the active site of superoxide dismutase (left y-axis and solid line) and the corresponding spin population differences (right y-axis and dashed line)

It is noteworthy that directed along the same trajectory as during the primary electron transfer in the active site of manganese superoxide dismutase (Fig. 2*a*), this time the superoxide ion bound to the proton of the hydroxyl group of the amino acid Tyr. This amino acid accompanied the superoxide ion throughout its path to manganese. This is shown by smeared minima 3 Å $\leq R \leq$ 5.5 Å. At the characteristic minimum R = 2.0 Å, the superoxide ion entered the manganese coordination sphere and completely replaced the water molecule. In this case, the superoxide ion formed two hydrogen bonds: with the water molecule and Tyr. As the calculation showed (Table 2), the hydroperoxide radical is in any case formed by splitting off a proton from water, and the second proton from Tyr forms a hydrogen peroxide molecule H_2O_2. Tyrosine is then protonated from the solvent and the cycle is completed. A sharp change in the difference between spin populations is within 2 Å $\leq R$. This criterion allows one to discard the variants of the associative and outer-sphere mechanisms and consider only the substitution mechanism. The donor radius is estimated as the sum of the average distance from the manganese atom to the histide ligands (2.031 Å) and the covalent radius of the nitrogen atom (0.71 Å).

A completely different phenomenon is observed for the case of iron superoxide dismutase. Two characteristic minima are observed. The first minimum R_1 = 4.3 Å is due to the stabilization of the system by the formation of two hydrogen bonds from the superoxide ion (to the water molecule and to the histidine ligand). This reflects the outer-sphere mechanism of secondary electron transfer. The second minimum R_2 = 2.1 Å is due to the stabilization of the system by the incorporation of the hydroperoxide radical into the first iron coordination sphere to form an octahedral structure. A sharp change in the difference of spin populations is within 3.4 Å $\leq R \leq$ 6 Å. This criterion allows us to discard the variant of the associative mechanism and consider only the outer-sphere mechanism. The donor radius is estimated as the sum of the distance from the iron atom to the hydroxide ion (2.114 Å) and the Van der Waals radius of the oxygen atom (1.55 Å).

Table 4 shows changes in the Gibbs functions ΔG^0, reorganization energy λ_{tot}, and activation energy $\Delta G^{\neq}$, as well as estimates of the first and second order electron transfer rate constants in the framework of the Marcus paradigm for the secondary electron transfer from the active site to the hyrdroperoxide radical. The rate constants are given for non-adiabatic and adiabatic calculation options. The preferred option is in bold.

Table 4

Kinetic and thermodynamic characteristics according to Marcus of the secondary electron transfer from the Me-SOD active site to the hydroperoxide radical

Parameter	Substitution mechanism	Outer-sphere mechanism
	Mn-SOD	Fe-SOD
ΔG^0, eV	–0.927	–0.508
r_D, Å	2.723	3.664
r_A, Å	1.337	2.217
R, Å	2.00	4.24
λ_{tot}, eV	1.774	1.540
$\Delta G^{\neq}$, eV	0.089	0.159
H_{DA}, eV	0.2226	0.1754
k_{diff}, $M^{-1}\cdot s^{-1}$	$2.02\cdot10^9$	$2.02\cdot10^9$
k_{et} (k_{et}^{AD}), s^{-1}	$1.92\cdot10^{13}$ (**$2.73\cdot10^{11}$**)	$9.11\cdot10^{10}$ (**$1.68\cdot10^{10}$**)
k (k^{AD}), $M^{-1}\cdot s^{-1}$	$3.87\cdot10^{11}$ (**$5.50\cdot10^{9}$**)	$1.75\cdot10^{10}$ (**$3.22\cdot10^{9}$**)
k_{obs} (k_{obs}^{AD}), $M^{-1}\cdot s^{-1}$	$2.01\cdot10^{9}$ (**$1.48\cdot10^{9}$**)	$1{,}81\cdot10^{9}$ (**$1.24\cdot10^{9}$**)

Transitions in Mn^{2+}-SOD-O_2^- are transitions between the quintet ground (Qt0) and the quintet first excited (Qt1) state. Unlike Fe^{2+}-SOD-O_2^-, Mn^{2+}-SOD-O_2^- transfer involves α-electrons. The unpaired electrons of the Mn^{2+}-SOD active center and the O_2^- superoxide ion have oppositely directed spins. The transition in Fe^{2+}-SOD-O_2^- is a transition between the sextet ground (St0) and sextet first excited (St1) states. All two interactions are adiabatic due to the high value of the H_{DA} matrix element.

As shown earlier, tyrosine is an important element for secondary electron transfer in manganese superoxide dismutase, which directs the superoxide ion to manganese. Tyr is displaced from its equilibrium position, and after the transfer of a proton and an electron, it returns to its original position. This increases the inner-sphere reorganization energy compared to iron superoxide dismutase. The first proton is split off from the water molecule, and the hydroxide ion OH^- is formed, which is located at a distance from manganese, and the hydroperoxide radical in the first coordination sphere of manganese. After electron transfer, the hydroperoxide ion retains a strong inner-sphere bond with the Mn^{3+} manganese ion. The second proton is immediately split off from the phenol group Tyr. The resulting hydrogen peroxide H_2O_2 molecule is easily split off from Mn^{3+}, and the hydroxide ion returns to its original position. At the end of the Mn-SOD catalytic cycle, a proton from the solvent protonates the Tyr phenolate ion. If we consider the mechanism of primary electron transfer in Mn-SOD as an associative one, then it can be noted that the values of the reorganization and activation energies are close to those for the secondary electron transfer by the substitution mechanism. The rate constants for the secondary electron transfer are two orders of magnitude smaller, but are above the diffusion limit.

Unlike manganese Mn^{2+}, iron Fe^{2+} exhibits a lower tendency to form a complex with the hydroperoxide radical. Here, only the outer-sphere mechanism is mainly realized. Compared to the manganese ion, the superoxide ion binds to iron during the primary electron transfer at a greater distance (by 0.56 Å), and during the secondary electron transfer, it does not show the formation of a stable bond at all. This indicates that iron binds less well with small anions than manganese. The rate constants for the secondary electron transfer are an order of magnitude smaller, but are above the diffusion limit.

Next, we consider the features of the behavior of the electron density at the bonding critical points of the complex of the superoxide ion and the Me-SOD active site in various versions of the mechanism of binding the superoxide ion and the metal (Table 5).

After the primary electron transfer at the manganese ion, the hydroxide ion OH^- splits off a proton from Asp and becomes a water molecule H_2O. Water is weaker bound to Mn^{2+} than to Mn^{3+}. Therefore, here it became possible to completely replace the water molecule with the superoxide ion. The Mn–HO_2 bond is quite strong and comparable to the Mn–His and Mn–Asp bonds. The topological characteristics of bonds involving Fe are similar to those for Fe^{3+}-SOD. This indicates the possibility of the outer-sphere mechanism.

Table 5

Critical bonding points (3; –1) for secondary electron transfer in the Me-SOD donor-acceptor complex. Parameters ρ and Δρ are expressed in atomic units

Bond	Parameter	Substitution mechanism	Outer-sphere mechanism
		Mn-SOD	Fe-SOD
Me–N^1	ρ	0.0795	0.0600
	Δρ	+0.311	+0.255
Me–N^2	ρ	0.0811	0.0748
	Δρ	+0.318	+0.347
Me–N^3	ρ	0.0880	0.0703
	Δρ	+0.352	+0.293
Me–O^{Asp}	ρ	0.0759	0.0764
	Δρ	+0.347	+0.339
Me–H_2O	ρ	–	0.0633
	Δρ		+0.279
Me–$O_2^-(HO_2)$	ρ	0.0893	–
	Δρ	+0.323	

Conclusions

Before the primary electron transfer from the solvent, a proton in the form of hydronium ion H_3O^+ enters the active site of Me^{3+}-SOD, which protonates the hydroxide ion OH^- to the water molecule H_2O. Due to the high chemical affinity of the Mn^{3+} ion with the strong hydroxide ligand and the low polarizing effect of the manganese ion, the water molecule splits off the proton to form the hydroxide ion. The proton passes to the carbonyl oxygen atom of the aspartate ion at manganese.

The primary electron transfers from the superoxide ion to the Mn^{3+}-SOD and Fe^{3+}-SOD active sites occur according to the associative mechanism. This indicates a high chemical affinity between the negatively charged superoxide ion and the positively charged metal ion. Substitution of the water molecule or the aspartate ion is not observed. The primary electron transfer precursor complex has an octahedral structure. The superoxide O_2^- ion binds more strongly to the Mn^{3+} ion with an electron transfer distance of 1.95 Å than to the Fe^{3+} ion with a transfer distance of 2.56 Å. The primary electron transfer for manganese superoxide dismutase by the associative mechanism has the reorganization energy of 1.840 eV and the activation energy of 0.065 eV with an energy release of 0.695 eV. The primary electron transfer for iron superoxide dismutase by the associative mechanism has the reorganization energy of 2.114 eV and the activation energy of 0.015 eV, which means a practically activationless transfer. The release of energy in this case is 1.109 eV. According to the values of the transfer rate constants in the case of Fe^{3+}-SOD, the elementary stage of electron transfer is an order of magnitude faster than in the case of Mn^{3+}-SOD.

Due to the instability of the O_2^{2-} peroxide ion, the secondary electron transfer is coupled with the proton transfer. It is unambiguous that the source of the proton is the water molecule. The proton is split off from the fifth ligand at the metal ion to form the hydroxide ion OH^-. The superoxide ion accepts the proton and becomes the peroxide radical $HO_2\cdot$. This is achieved by the active interaction of the superoxide ion and the water molecule. The mechanisms of secondary electron transfer are significantly different for Mn^{2+}-SOD and Fe^{2+}-SOD. In manganese superoxide dismutase, the superoxide ion forms a hydrogen bond with the hydroxyl group of tyrosine. Secondary electron transfer in manganese superoxide dismutase occurs by substitution mechanism at a distance of 2.0 Å. The transfer has the reorganization energy of 1.774 eV and the activation energy of 0.089 eV with an energy release of 0.927 eV. In iron superoxide dismutase, the superoxide ion combines with the water molecule and the histidine ligand at a distance of 4.24 Å from iron. The transfer has the reorganization energy of 1.540 eV and the activation energy of 0.159 eV with an energy release of 0.508 eV. According to the values of the transfer rate constants in the case of Mn^{2+}-SOD, the elementary stage of electron transfer is somewhat faster than in the case of Fe^{2+}-SOD.

References

1 Barja, G. (1999). Mitochondrial Oxygen Radical Generation and Leak: Sites of Production in States 4 and 3, Organ Specificity, and Relation to Aging and Longevity. *J. Bioenergetics and Biomembranes*, *31*, 347–366. https://doi.org/10.1023/A:1005427919188

2 Cabelli, D.E., Riley, D., Rodriguez, J.A., Valentine, J.S. & Zhu, H. (1999). Models of superoxide dismutases. Biomimetic Oxidations Catalyzed by Transition Metal Complexes. *Imperial College Press*, 461–508. https://doi.org/10.1142/9781848160699_0010

3 Fridovich, I. (1997). Superoxide anion radical (O_2^-), superoxide dismutase and related matters. *J. Biol. Chem.*, *272*, 18515–18517. https://doi.org/10.1074/jbc.272.30.18515

4 Azadmanesh, J. & Borgstahl G.E.O. (2018). A Review of the Catalytic Mechanism of Human Manganese Superoxide Dismutase. *Antioxidants, 7, 25.* https://doi.org/10.3390/antiox7020025

5 Lah, M. S., Dixon, M. M., Pattridge, K. A., Stallings, W. C., Fee, J. A. & Ludwig, M. L. (1995). Structure-function in Escherichia coli iron superoxide dismutase: comparisons with the manganese enzyme from Thermus thermophilus. *Biochemistry*, *34*(5), 1646–1660. https://doi.org/10.1021/bi00005a021

6 Marcus, R.A. & Sutin, N. (1985). Electron transfers in chemistry and biology. *Biochimica et Biophysica Acta*, *811*, 265–322. https://doi.org/10.1016/0304-4173(85)90014-x

7 Neese, F. (2012). The ORCA program system. *Wiley interdisciplinary Reviews — Computational Molecular Science*, *2*(1), 73–78. https://doi.org/10.1002/wcms.81

8 Perdew, J.P., Burke, K. & Ernzerhof, M. (1996). Generalized Gradient Approximation Made Simple. *Phys. Rev. Letters*, *77*, 3865. https://doi.org/10.1103/physrevlett.77.3865

9 Weigend, F. & Ahlrichs, R. (2005). Balanced basis sets of split valence, triple zeta valence and quadruple zeta valence quality for H to Rn: Design and assessment of accuracy. *Phys. Chem. Chem. Phys*., *7*, 3297. https://doi.org/10.1039/b508541a

10 Xerri, B., Petitjean, H., Dupeyrat, F., Flament, J.-P., Lorphelin, A., Vidaud, C. et al. (2014). Mid- and Far-Infrared Marker Bands of the Metal Coordination Sites of the Histidine Side Chains in the Protein Cu, Zn-Superoxide Dismutase. *European Journal of Inorganic Chemistry*, *2014*(27), 4650–4659. https://doi.org/10.1002/ejic.201402263

11 Caldeweyher, E., Bannwarth, C. & Grimme, S. (2017). Extension of the D3 dispersion coefficient model. *J. Chem. Phys*., *147*, 034112. https://doi.org/10.1063/1.4993215

12 Cossi, M., Rega, N. & Scalmani, G. et al. (2003). Energies, structures and electronic properties of molecules in solution with the C-PCM solvation model. *Chem. Phys.*, *24*, 669–681. https://doi.org/10.1002/jcc.10189

13 Ryabykh, A.V., Maslova, O.A., Beznosyuk, S.A. & Masalimov, A.S. (2022). The Role of Zinc Ion in the Active Site of Copper-Zinc Superoxide Dismutase. *Bulletin of the University of Karaganda — Chemistry, 106(2), 77-86.* https://doi.org/10.31489/2022Ch2/2-22-20

14 Alexandrov, I.V. (1980). Physical aspects of charge transfer theory. *Chemical Physics*, *51*(3), 449–457.

15 Cordero, B., Gómez, V., Platero-Prats, A. E., Revés, M., Echeverría, J., Cremades, E., Barragán, F. & Alvarez, S. (2008). Covalent radii revisited. *Dalton Transactions*, (21), 2832–2838. https://doi.org/10.1039/B801115J

16 Batsanov, S.S. (2001). Van der Waals radii of elements. *Inorganic materials*, *37*(9), 871–885. https://doi.org/10.1023/A:1011625728803

17 Eberson, L. (1985). The Marcus theory of electron transfer, a sorting device for toxic compounds. *Advances in Free Radical Biology & Medicine*, *1*(1), 19–90. https://doi.org/10.1016/8755-9668(85)90004-3

18 Rosso, K.M. & Rustad, J.R. (2000). Ab initio calculation of homogeneous outer sphere electron transfer rates: application to $M(OH_2)_6^{3+/2+}$ redox couples. *The Journal of Physical Chemistry A*, *104*(29), 6718–6725. https://doi.org/10.1021/jp994164h

19 Lu, T. & Chen, F. (2012). Multiwfn: A multifunctional wavefunction analyzer. *Journal of computational chemistry*, *33*(5), 580–592. https://doi.org/10.1002/jcc.22885

Information about authors*

Ryabykh, Andrey Valerievich — Assistant and Engineer, Department of Physical and Inorganic Chemistry, Altai State University, Lenin avenue, 61, 656049, Barnaul, Russia; e-mail: ryabykh@chem.asu.ru; https://orcid.org/0000-0003-3699-3932

Maslova, Olga Andreevna — Candidate of Physical and Mathematical Sciences, Associate Professor, Physical and Inorganic Chemistry Department, Altai State University, Lenin avenue, 61, 656049, Barnaul, Russia; e-mail: maslova_o.a@mail.ru; https://orcid.org/0000-0003-3862-3687

Beznosyuk, Sergey Alexandrovich (*corresponding author*) — Doctor of Physical and Mathematical Sciences, Professor, Head of the Physical and Inorganic Chemistry Department, Altai State University, Lenin avenue, 61, 656049, Barnaul, Russia; e-mail: bsa1953@mail.ru; https://orcid.org/0000-0002-4945-7197

*The author's name is presented in the order: *Last Name, First and Middle Names*